The Measure of TiO_2 Photocatalytic Efficiency and the Comparison of Different Photocatalytic Titania

Yikui Du[†] and Joseph Rabani*[,‡]

Department of Physical Chemistry, The Hebrew University of Jerusalem, Jerusalem 91904, Israel

Received: May 28, 2003; In Final Form: July 3, 2003

The dependence of hydroxyl radical yield on the substrate concentration, pH, oxygen concentration, and light intensity, using different TiO_2 preparations, was investigated. The quantum yields of formaldehyde and carbon dioxide, obtained with the aid of an integrating sphere in the methanol and formate systems, respectively, were used to derive the primary yield of hydroxyl radicals. The limiting yield of $^{\bullet}OH_{ads}$, achieved at high scavenger concentrations, is independent of the nature of the scavenger (methanol or formate) and is nearly constant in the range $1 < pH < 12$. While the presence of air induces a 15-fold increase in product yield, compared to air-free systems, further increase of oxygen concentration has only a small effect. The effect of changing the $^{\bullet}OH$ scavenger concentration, pH, and light intensity corresponds to simple competition between pseudo first- and second-order reactions. Under the conditions of the present work the scavengers CH_3OH, HCO_2^- and HCO_2H react only with the hydroxyl radical, not with its precursor hole. Hydrogen peroxide, which is produced in the above systems upon reduction of oxygen by both TiO_2 electrons and the organic free radicals, is further reduced to $^{\bullet}OH$ radicals, doubling the products yield. A rigorous treatment of the effect of absorbed photon density on the quantum yield, based on the simple square root dependency, enables the derivation of a constant, K_d, which is related to the efficiency of surface water oxidation to hydroxyl radicals, relative to the electron hole recombination at the given pH and oxygen concentration. This parameter is a property of the TiO_2, and is not affected by the experimental conditions such as wavelength and layer thickness. Comparison of K_d using different types of TiO_2 shows that in contrast to commonly assumed, preparation methods and sizes of aged titanium dioxide nanoparticles have only a relatively small effect on the basic photocatalytic efficiency. Comparison of the quantum yield in TiO_2 layers to results in aqueous suspensions using similar photon flux shows moderate differences. The results are discussed in view of the much larger absorbed photon density in the suspended nanoparticles combined with much larger volume in the bulk of the solution.

Introduction

A growing interest in photoelectrochemistry and photocatalytic oxidation of organic compounds follows the pioneering works of Gerischer,[1] and Fujishima and Honda.[2] Photocatalytic detoxification of organic pollutants with the aid of TiO_2 particles or layers is a promising tool for purification and sterilization of environmental aqueous media.[3−9] Absorption of a photon with energy greater than the band gap energy results in the formation of conduction band electron and valence band hole, according to reaction 1. It is commonly accepted that the hole is quickly converted to the hydroxyl radical upon oxidation of surface water, according to reaction 2, which competes with the recombination reaction 3. The hydroxyl radical is the major reactant responsible for oxidation of organic substrates. Convincing evidence for the generation of $^{\bullet}OH_{ads}$ (as well as bulk $^{\bullet}OH$) by TiO_2 photolysis has been obtained from photochemical and radiation chemical studies of $^{\bullet}OH$ and $^{\bullet}OH_{ads}$ addition to phenol compared to electron-transfer oxidation of phenol by TiO_2 holes and by strong oxidants,[10] spin trapping techniques, using $^{\bullet}OH$ scavengers to produce a free radical,[11−15] or using a stable free radical scavenger for $^{\bullet}OH$.[16] Knowledge of the yield of the $^{\bullet}OH$ radical and the factors affecting this yield and the related product yields in the presence of substrates is essential for comparison of photocatalytic activities of different TiO_2 photocatalysts.

The literature concerning TiO_2 holes and $^{\bullet}OH_{ads}$ often refers to both as "holes" without discrimination, although the term "localized" or "trapped" holes is in some cases implicitly used for $^{\bullet}OH_{ads}$. The TiO_2 electrons may react in the form of conduction band excess electrons, or first become trapped at the TiO_2 surface by adsorbed dopants, surface defects, or added solutes. In the presence of oxygen, $e_{TiO_2}^-$ is converted to a superoxide radical according to reaction 4. Since reaction 4 is relatively slow, it is expected to be followed by the faster reaction 5, followed by reaction 6.[17]

In the presence of an organic solute, RH_2, hydrogen abstraction according to reaction 7 takes place. Many materials may react with both h^+ and $^{\bullet}OH_{ads}$ (as well as other trapped $^{\bullet}OH$). However, the TiO_2 photocatalysis is complicated by the confinement of the reactions of the primary active species, $e_{TiO_2}^-$, h^+, $^{\bullet}OH_{ads}$, and possibly others to the nanocrystallite surface. The second-order scavenging reactions of scavengers compete with inhomogeneous radical−radical reactions, which usually depend on the local concentrations at the surface. Therefore, the product

* Corresponding author.
[†] E-mail: duyk@vms.huji.ac.il.
[‡] E-mail: rabani@vms.huji.ac.il.

10.1021/jp035491z CCC: $25.00
Published on Web 10/04/2003

yields depend not only on the nature of the scavenger, photocatalyst, surface area, and reactant concentration, but also on the light intensity.[18−44]

$$TiO_2 \xrightarrow{h\nu} e_{TiO_2}^- + h^+ \quad (1)$$

$$h^+ + H_2O_{ads} \rightarrow {}^\bullet OH_{ads} \quad (2)$$

$$h^+ + e_{TiO_2}^- \rightarrow TiO_2 \quad (3)$$

$$e_{TiO_2}^- + O_2 \rightarrow {}^\bullet O_2^- \quad (4)$$

$${}^\bullet O_2^- + e_{TiO_2}^- (+ 2H^+) \rightarrow H_2O_2 \quad (5)$$

$$e_{TiO_2}^- + H_2O_2 \rightarrow {}^\bullet OH + OH^- \quad (6)$$

$${}^\bullet OH_{ads} + RH_2 \rightarrow H_2O + {}^\bullet RH \quad (7)$$

$${}^\bullet CH_2OH + O_2 \rightarrow {}^\bullet O_2CH_2OH \quad (8)$$

$${}^\bullet CO_2^- + O_2 \rightarrow {}^\bullet O_2^- + CO_2 \quad (9)$$

$${}^\bullet O_2CH_2OH \rightarrow {}^\bullet O_2^- + HCHO + H^+$$

or

$$\rightarrow HO_2^\bullet + HCHO \quad (10)$$

$${}^\bullet O_2^- + {}^\bullet O_2^- + 2H^+ \rightarrow O_2 + H_2O_2 \quad (11)$$

$${}^\bullet O_2^- + H_2O_2 \rightarrow {}^\bullet OH + OH^- + O_2 \quad (12)$$

$${}^\bullet OH + e_{TiO_2}^- (+ H^+) \rightarrow TiO_2 + H_2O \quad (13a)$$

$${}^\bullet OH + {}^\bullet RH \rightarrow H_2O + R \quad (13b)$$

$${}^\bullet OH + {}^\bullet O_2^- (+ H^+) \rightarrow H_2O + O_2 \quad (13c)$$

In a typical organic substrate in aqueous solution, the $^\bullet RH$ radical, produced by reaction 7, reacts with oxygen and produces a peroxy radical (e.g., in the case of methanol)[45] or a superoxide radical (e.g., in the case of formate),[46] according to reactions 8 and 9, respectively. In the case of methanol, the peroxy radical produces the superoxide radical and formaldehyde according to reaction 10, which is catalyzed by bases.[45] Many other peroxy radicals, however, are stable with respect to decomposition into an oxidation product and superoxide.

Dismutation of $^\bullet O_2^-$ in the bulk takes place (reaction 1) via disproportionation of $^\bullet O_2^-$ with $HO_2^\bullet$, in competition with reaction 5. $HO_2^\bullet$ has a pK at 4.8.[46,47] When the pH is considerably below the pK, the dismutation involves two $HO_2^\bullet$ radicals. The peroxy radical may also react with hydrogen peroxide according to the Haber-Weiss reaction 12. However, the competition between reactions 5, 6, 11, and 12 does not affect the overall material balance. The product yield, Φ_P, where P stands for formaldehyde and CO_2, in the methanol and formic acid/formate systems, respectively, is given by: $\Phi_P = 2\Phi_{OH} - \Phi_{H_2O_2}$.

Although the above mechanism is strongly supported by photolysis and radiation chemical data, key reactions are often ignored in the interpretation of photocatalysis results. Furthermore, in the absence of agreed standard conditions, results from different laboratories and even results from the same laboratory are not used for broad comparative studies, and there is no quantitative procedure, which enables predictions of photocatalytic results on the basis of fundamental yields, reaction rate constants and adsorption information. This is particularly the case when different procedures for preparation of TiO_2 are involved. Even in the cases where quantum yields are reported,[30,37−44,48] Φ cannot serve as a general measure for the photocatalytic quality of the photocatalyst because it changes with the specific working conditions such as added solute, solute concentration, wavelength of illumination, layer thickness, light intensity, as well as suspension and sol concentrations. The diverging results, particularly when different laboratories are compared, led to the common assumption that the properties of TiO_2 nanocrystallites strongly depend on accidental impurities and may change by minor uncontrolled variation of conditions.

In the present manuscript we report a comparative study of different TiO_2 preparations and nanocrystallite sizes, obtained from different companies, under a wide range of conditions. For this purpose, high concentrations of organic additives, which produce intermediates yielding superoxide radicals upon reaction with oxygen, were used to determine the yield of hydroxyl radicals. Carefully correcting for scattered light and taking into account the inhomogeneous distribution of the absorbed photon density leads to a surprising similarity of all tested TiO_2 samples. The scope of the work was limited to aged TiO_2 nanoparticles, where the surface defects have reached a stable level, excluding Q-particles. A preliminary study under the above limiting conditions has been reported recently.[49]

Experimental Section

Materials. NaOH (Frutarom), $HClO_4$ (Baker), HCl (Baker), Na_2HPO_4 (Sigma), NaH_2PO_4 (BDH), Na_2CO_3 (Baker), $NaHCO_3$ (Frutarom), formic acid (Baker), and sodium formate (Riedel-de Haen) were used as received. Phosphate buffer (0.03 M) was used to adjust the pH between 7 and 9. Carbonate/bicarbonate (0.012 M) was used between pH 9 and 11, while pH's >11 were adjusted using NaOH. An Orion Ross combination glass electrode was used for pH measurements, (± 0.01 pH units at 25 °C).

The following TiO_2 nanocrystallites have been studied:

(1) S5-300A, aqueous dispersion 15% w/w in solution pH 1, product of Millenium Inorganic Chemicals, aggregate diameter 40−80 nm, surface area 250 m^2/g.

(2) S5-300B, aqueous dispersion 15% w/w in solution pH 11, product of Millenium Inorganic Chemicals, aggregate diameter 40−80 nm, surface area 250 m^2/g.

(3) Degussa P-25 powder, primary diameter 20 nm, surface area 75 m^2/g.

(4) STS-01, product of Ishihara, 40% suspension in acidic solution, aggregate diameter 60 nm (primary particle diameter 7 nm), 300 m^2/g.

(5) STS-21, product of Ishihara, 40% suspension in alkaline solution, aggregate diameter 200 nm (primary particle diameter 20 nm), 50 m^2/g.

(6) Colloidal solution prepared by hydrolysis of titanium 2-propoxide (Aldrich), [50] using a slightly modified procedure.[49] The resulting suspension was heated at pH 2.5 (HNO_3) for several days at 80° C until a clear solution was obtained yielding nanocrystallites with average diameter of 5 nm, with surface area 300 m^2/g. Solutions contained 18% w/w TiO_2.

(7) TiO_2 nano tubes, prepared with the aid of sonolysis, generously donated by Prof. A. Gedanken,[51] surface area 600 m^2/g.

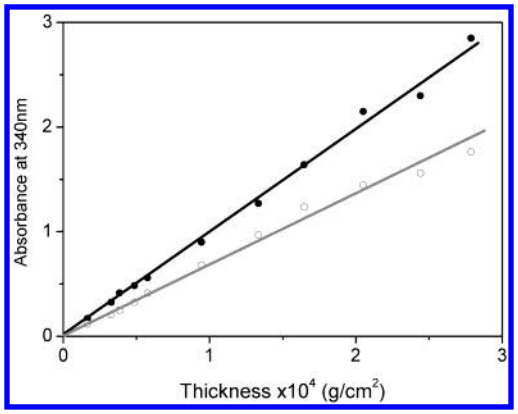

Figure 1. Corrected absorbance vs apparent measured absorbance STS-21 type TiO_2. The open circles represent values measured with the aid of a spectrophotometer and corrected for scattered light. The closed circles show the uncorrected absorbance. The supporting plate, with or without the TiO_2 layer, was immersed in water in a cuvette well inside the integrating sphere.

(8) TiO_2 photocatalyst in the form of porous pellets, product of Sachtleben Chemie.

With the exception of the latter, all TiO_2 samples were immobilized on ITO or glass (same results) by successive spin coatings. Layer dimensions were $(0.8 \pm 0.05) \times (2.5 \pm 0.1)$ cm^2.

Illumination. The excitation light source was a 75 W Xe lamp. The light was filtered by Pyrex glass (2 mm thick, cutting below 300 nm) and ORIEL 59800 cutoff filter (transmitting below 400 nm). The light intensity was adjusted by appropriate neutral density filters, and was monitored by an OPHIR NOVA 10A-P-SH light detector during illumination to ensure stability of the light. A water filter (9.5 cm) was used to minimize heating by the IR irradiation. Interference filter transmitting at 333, 340, or 350 nm were used in order to obtain monochromatic light.

The Illumination Cell. Experiments were carried out in a closed $1 \times 1 \times 5$ cm^3 cell with Pyrex windows containing 3 cm^3 solution. The TiO_2 was usually used as a layer on ITO or glass, with dimensions 0.85×2.5 cm^2, while the illumination area had dimensions of 0.4×1.5 cm^2. Usually, air-saturated 2 M methanol or 0.1 M formic acid/formate was used as an $^{\bullet}OH$ scavenger. The TiO_2 layer was near to the optical window from which the light entered, with the TiO_2–coated side facing the solution. The layer was preequilibrated with the solution in the dark by mixing (magnetic stirrer) for 10 minutes prior to illumination. Mixing continued during illumination as well as 5 minutes after the illumination.

Formaldehyde was determined by the Nash method,[52] based on the Hantzsch reaction: 15 μL of acetylacetone was added to 3 mL of solution, consisting of 1.5 mL of sample and 1.5 mL of 0.18 M ammonium phosphate buffer at pH 6.0. Spectrophotometric measurements were carried out at 412 nm ($\epsilon = 8000$ M^{-1} cm^{-1}) using Kontron's Uvikon 860 spectrophotometer.

The amount of absorbed light was determined from the decrease in light intensity observed upon replacing a bare ITO glass with one coated with TiO_2, using the Fe^{3+} oxalate actinometer.[53,54] Absorbed light in scattering TiO_2[55−58] was measured with the aid of an integrating sphere, product of Labsphere, 15 cm diameter, using an Ophir Optronics detector model PD300-UVSH. Typical results for corrected vs measured absorbance is shown for STS-21 type TiO_2 in Figure 1. Corrected absorbance have been derived as follows: the absorbance of the TiO_2 layer was first measured in a cuvette filled with water using a spectrophotometer, where the apparent absorbance, "D"$_{sol}^{340} = \log($"I_0"$/I_t)$ includes also the scattered light. The difference between the apparent and corrected absorbance, D_{sol}^{340}, results from the part of the analyzing light, namely, the scattered light not reaching the detector, while all the analyzing light is measured at the reference port. The corrected absorbance is given by $D_{sol}^{340} = \log(I_0/(I_{scat} + I_t))$, where I_0 is the light intensity detected in the absence of the TiO_2 layer, I_{scat} is the light intensity, which does not reach the detector due to scattering, and I_t is the light intensity which is transmitted through the TiO_2 layer reaching the detector. Since the detector is separated from the sample by about 10 cm, the measured transmitance T is separated from scattered light. This was verified by light signal measurements where the detector was placed 10 cm behind the tested sample, showing the same value for transmittance. The fraction of scattered light is measured in the integrating sphere as $T_{scat} = I_{scat}/I_0$ by the relative signal (nW) in the presence and absence of the TiO_2 layer. T_{scat} was corrected for the fraction of the light, which is reabsorbed by the TiO_2, T_{reads}. T_{reads} was measured using a 2 mm cell instead of the TiO_2 layer, with TiO_2 suspension or other solution, the absorption of which, at the given wavelength, is equal to that of the respective TiO_2 layer. For the determination of T_{reads}, the 2 mm cuvette is positioned outside the direct light path so that only light reflected from the wall of the integrating sphere can be absorbed. T_{reads} is equal to the ratio between the light intensities in the presence and absence of the absorbing material.

CO_2 was determined using Hewlett-Packard GC model 5890 with He gas carrier.

Results and Discussion

The limiting yield of a two-electron oxidation product, observed at high scavenger concentrations, is directly related to the maximum yield of $^{\bullet}OH$ radicals under the experimental conditions of pH and light intensity. This yield is determined by the competition between reaction 2 and 3, and is not expected to depend on the nature of the $^{\bullet}OH$ scavenger used. Qualified scavengers must discriminate between $^{\bullet}OH$ radicals and other forms of holes, mobile or localized.

Two scavengers have been used in the present work, namely, methanol and formic acid/formate. Formation of HCHO in the methanol system has been previously reported to increase nearly linearly with the time of illumination under the conditions used in this work, while the apparent rate of formation reaches plateau at $[CH_3OH] > 2$ M.[49] The previous work, however, was limited to one type of TiO_2 preparation and to near neutral and basic pH. Expanding the previous work to acid pH requires the knowledge of the fate of the $^{\bullet}O_2CH_2OH$ radical, under the acid conditions, where fast decomposition according to reaction 10 is not guaranteed. Indeed, measurements of γ-radiation yields of HCHO in air-saturated 5 mM methanol resulted in G_{HCHO} values ranging from 0.8 at pH 0.4 (1 M $HClO_4$) to 2.3 at pH 4.8 and 2.7 at pH = 7 (Figure 2). Under the experimental conditions, methanol scavenges all the $^{\bullet}OH$ radicals but only a negligible fraction of the hydrogen atoms. The latter react almost exclusively with the dissolved oxygen. Therefore $G_{HCHO} = 2.7$ is expected if all $^{\bullet}O_2CH_2OH$ radicals decompose according to reaction 10. Consequently, other decomposition routes become open in acid solutions and therefore the use of the methanol system becomes complicated for determination of Φ_{OH} in acid media. The formic acid/formate system has been therefore used below pH 6 to supplement the methanol data. This system produces $^{\bullet}CO_2^-$ or $HCO_2^{\bullet}$ free radical upon reaction with the

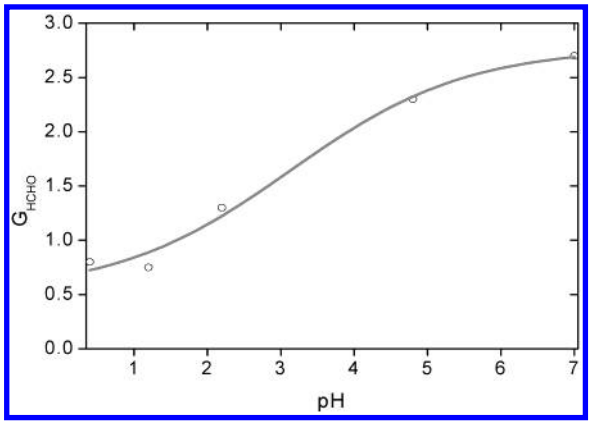

Figure 2. Formation of formaldehyde by radiolytic oxidation of aerated methanol solution 5×10^{-3} M CH_3OH, 9.23 Gy/min. (total dose 380 Gy) Cs^{137} γ-rays, pH adjusted using $HClO_4$ (pH 0−2.2), acetate buffer (pH 4.8, total concentration 2 mM), and phosphate buffer (pH 7, total buffer concentration 10 mM).

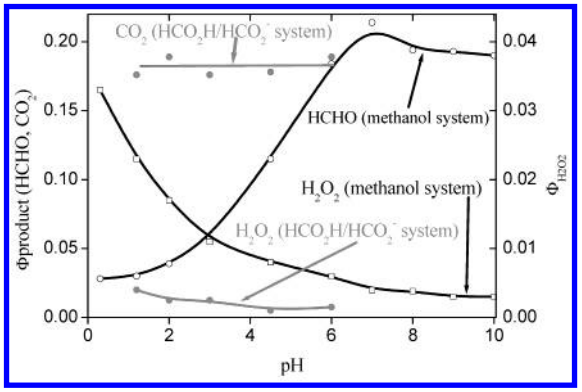

Figure 3. $\Phi_{H_2O_2}$, Φ_{HCHO} and Φ_{CO_2} TiO_2 type STS-01 ($D_{340} = 1.2$), 1.3×10^{-9} ein/s (1.05×10^{-5} ein s^{-1} g^{-1}), 340 nm interference filter, 2 M CH_3OH or 0.2 M HCO_2H/HCO_2^- aerated solutions. Illumination time: 60 min.

hydroxyl radical, which further reacts with oxygen according to reaction 7 (or the parallel reaction involving $^{\bullet}CO_2H$) in the entire pH range. The end product of the reaction is CO_2. Although the latter system can be used to determine Φ_{OH} at both acid and alkaline media, the presence of CO_2 as a common impurity in alkaline solutions is a disadvantage. We have therefore used predominantly methanol at pH > 6 and formic acid/formate at pH < 6, although whenever comparative tests were carried out (see later), the calculated quantum yields of $^{\bullet}OH$ radicals are similar in both systems.

The Effect of pH on Φ_{OH}. The effect of pH on product yields in the methanol and the formic acid/formate system, respectively, is presented in Figure 3. The decrease of Φ_{HCHO} in acid pH, which is in part associated with the stabilization of O_2CH_2OH with respect to reaction 10 (see discussion of Figure 2), parallels the radiolytic results (Figure 2). The decrease, however, is sharper in photolysis. Part of this difference is related to the increase in $\Phi_{H_2O_2}$ in the photolytic system. While in the radiolytic system, oxygen protects hydrogen peroxide by its efficient reaction with the reducing radicals (CH_2OH, H and e_{aq}^-), the relatively slow reaction 4 compared to reactions 5 and 6[17] results with partial or total destruction of hydrogen peroxide. These reactions are expected to double Φ_{HCHO}, if all the peroxide molecules are reduced to $^{\bullet}OH$ radicals. Other reactions of $e_{TiO_2}^-$ with intermediates such as $^{\bullet}O_2CH_2OH$ and $HO_2^{\bullet}$ and of $^{\bullet}CH_2OH$ with H_2O_2 provide additional paths for elimination of hydrogen peroxide along with parallel doubling of the formaldehyde yield. From Figure 3 it is obvious that even in acid solutions of methanol, where the residual concentration of hydrogen peroxide is highest, it has only a marginal effect on the overall material balance. Consequently, the difference in the slope of HCHO building up between the radiolytic and photolytic systems must be in part due to the presence of TiO_2 in the latter, so that the relevant reaction rates at the TiO_2 surface differ from the bulk rates. Because of this, formic acid/formate was introduced as a substitute for methanol in the acid range. Figure 3 shows that the CO_2 yield in the formic acid/formate system does not depend on pH in the range studied. Note that the use of formate in alkaline solutions was avoided because of the inaccuracy introduced by initially present CO_2. However, at pH 6, where both methanol and formate can be used for the determination of quantum yields, $\Phi_{HCHO} = \Phi_{CO_2}$, suggesting that the methanol and formic acid/formate systems together are qualified to provide information on Φ_{OH} in the entire pH range. Note that $\Phi_{H_2O_2}$ (formic acid/formate) $\ll \Phi_{H_2O_2}$ (methanol) (Figure 3). This indicates that at least CO_2^-/CO_2H and perhaps also $^{\bullet}CH_2OH$ may react with H_2O_2 despite the presence of excess oxygen. Such reaction, however, does not affect the overall material balance. Previous determinations of the quantum yield [48,59] in the formic acid−formate system were apparently carried out at scavenger concentrations, which do not guarantee total $^{\bullet}OH$ radical scavenging, and therefore cannot be compared to the values reported here.

The similar limiting product yields in both methanol and formic acid/formate systems indicate that in both cases the scavenger reacts with all the $^{\bullet}OH$ radicals but not with holes. This conclusion is in agreement with the earlier work on electrolytic generation of $^{\bullet}OH$ radicals from Nb-doped TiO_2 holes, showing that formate degrades primarily via a hydroxyl radical mechanism.[60] The measurements of limiting initial quantum yields, which are independent of the scavenger, enable comparison between different TiO_2 preparations without relating to specific conditions such as concentrations, adsorption, or secondary reactions. The observation that $\Phi_{HCHO} = \Phi_{CO_2}$ (HCO_2^-) $= \Phi_{CO_2}$ (HCO_2H) suggests that the oxidation products HCHO and CO_2, respectively, represent reactions of $^{\bullet}OH$ radicals as opposed to direct hole-scavenging. In addition, we found no evidence for parallel degradation paths,[48] and reaction 7 followed by reaction 9 (or an analogous reaction involving HCO_2H) represents the only path for formic acid/formate oxidation to CO_2 under our conditions.

Figure 4 shows that while at pH 2 a limiting yield is achieved at 0.02 M formic acid, the formate ion requires somewhat higher concentration. Since the reaction rate of formate ions with $^{\bullet}OH$ radicals is about 25 times higher than the respective rate of the un-dissociated acid,[61,62] the observed difference must be attributed to differences in adsorption of HCO_2H and HCO_2^-. The preferential adsorption of the undissociated acid is in contrast with gas-phase results, which show that adsorption of formic acid by TiO_2 is dissociative, and consequently the adsorption of HCO_2^- is stronger than HCO_2H.[63−65] This apparent discrepancy is probably related to the difference in solvation energies between the acid and its anion. Comparison between the formic acid/formate and methanol systems shows that relatively much higher methanol concentrations are required to reach the plateau of HCHO yield, although the rate of reaction 7 is 7 times faster for methanol, compared to formic acid.[61,66] Again, these results can be rationalized by the relatively strong adsorption of the acid.

In conclusion, the similar results obtained with methanol and formate at pH 6, and the similar quantum yields in the formate/formic acid system at pH 2 and 6 show that (a) The measured

TABLE 1: Comparison between 333 and 350 nm Light Measured in STS-01 Layers at pH 7 (10 mM total phosphate) Using 2 M CH_3OH. Φ_{OH} Includes OH Radicals Obtained via Reduction of O_2. Values of Φ_{OH} Were Corrected for Scattered Light

absorbance of TiO_2	abs. light intensity (ein/s)	abs. light density (ein s^{-1} g^{-1})	Φ_{HCHO}	K_I $s^{1/2}/ein^{-1/2}$	$K_I(g)$ $s^{1/2}$ $g^{1/2}$ $ein^{-1/2}$ [a]	$K_I(V)$ $s^{1/2}$ $cm^{3/2}$ $ein^{-1/2}$ [b]
$D_{333} = 0.9$	3.5×10^{-11}	5.65×10^{-7}	0.67	3.3×10^5	2.6×10^3	1.6×10^3
$D_{350} = 0.9$	3.5×10^{-11}	1.77×10^{-7}	1.0	1.7×10^5	2.4×10^3	1.4×10^3

[a] Calculated as $K_I(g) = (\Phi(\lambda)^{-1} - \Phi_{max}(\lambda)^{-1}) \times \Phi_{max}(\lambda)(g/I)^{1/2}$, using $\Phi_{max} = 2$. Note that the layer extinction coefficient at 333 nm is 3 times higher that at 350 nm, and hence the thickness and weight are smaller by the same factor. [b] Calculated as $K_I(V) = (\Phi(\lambda)^{-1} - \Phi_{max}(\lambda)^{-1}) \times \Phi_{max}(\lambda)(V/I)^{1/2}$, using $\Phi_{max} = 2$.

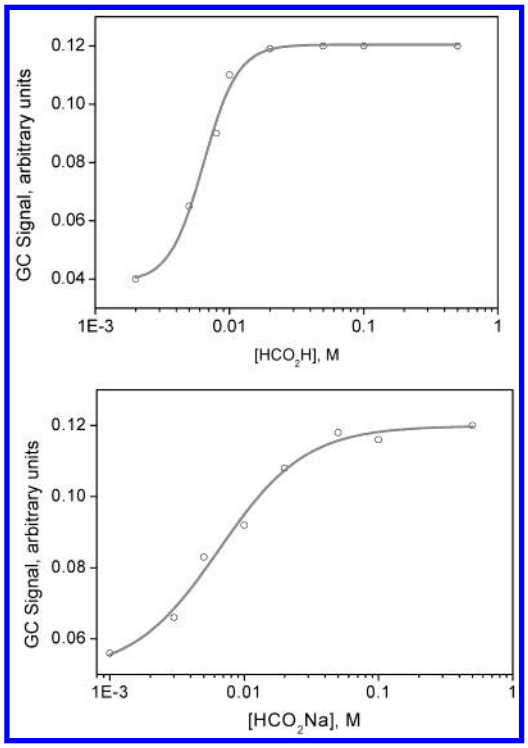

Figure 4. (a) Effect of formic acid concentration on the yield of CO_2. Absorbed light intensity 6.2×10^{-11} ein/s (8.2×10^{-7} ein s^{-1} g^{-1}), illumination time 30 min, pH 2 (HCl), STS-01 type TiO_2, $D_{sol}^{333} = 1.1$. (b) Effect of formate concentration on the yield of CO_2. Absorbed light intensity 6.2×10^{-11} ein/s (8.2×10^{-7} ein s^{-1} g^{-1}), illumination time 30 min, pH 6 (20 mM Na_2HPO_4 and 0.2 M NaH_2PO_4), STS-01 TiO_2, $D_{sol}^{333} = 1.1$.

yield is determined by the competition between reactions 2 and 3 only and does not depend on the nature of the scavenger used. (b) The quantum yield of •OH radicals, which in the formic acid/formate system is directly related to the yield of CO_2, does not depend on pH in the range 2−6. An earlier study using a different TiO_2 preparation[49] shows that Φ_{OH} is constant, within the experimental error of 20% in the pH range 7−12.

Effect of Light Intensity on Φ_{OH}. A square root decrease of quantum yield upon increasing illumination intensity has been proposed by Gerischer, [40,67] and observed by several groups,[22,23,38,41,68,69] although quantum yields independent of light intensity have been reported for low photon flux.[14,70] Under the conditions of the present work, Φ_{OH} and the light intensity I closely obey eq 14,[49] as demonstrated in Figure 5 for STS-01 type TiO_2.

$$1/\Phi_{exp}^{(\lambda,l,A,d)} = 1/\Phi_{max} + K_I^{(\lambda,l,A,d)} I^{1/2}/\Phi_{max} \qquad (14)$$

The quantum yield and K_I ($s^{1/2}$ $ein^{-1/2}$) depend on the excitation wavelength. Thus, different values are measured at 333 and 350 nm, when layers with the same absorbance are compared (Table 1). However, when the absorbed photon density (ein g^{-1} s^{-1} or ein cm^{-3} s^{-1}) is considered, similar $K_I(g)$ ($s^{1/2}$ $g^{1/2}$ $ein^{-1/2}$) and

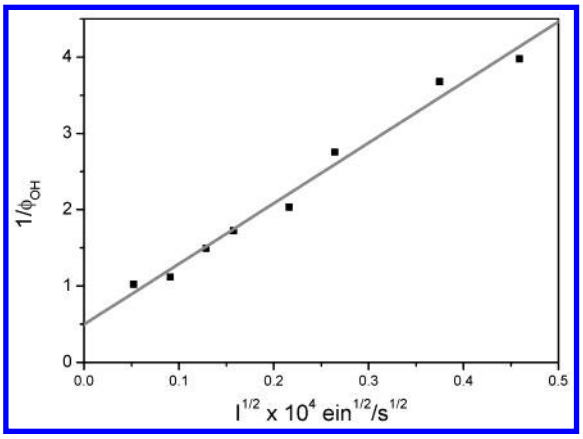

Figure 5. Increase of $1/\Phi_{OH}$ with the square root of light intensity. The results have been analyzed according to the eq 14, where $\Phi_{max} = 2.02$ (1.85 if not corrected for scattering) and $K_I = 1.60 \times 10^5$ $s^{1/2}/ein^{1/2}$. Measured in STS-01 layers at pH 7 (0.002 M Na_2HPO_4, 0.002 M NaH_2PO_4) using 2 M CH_3OH, 350 nm light, $D_{sol}^{350} = 0.93$, $W_A = 0.32$ mg/cm^2. Φ_{OH} includes OH radicals obtained via reduction of O_2.

$K_I(V)$ ($s^{1/2}$ $cm^{3/2}$ $ein^{-1/2}$) values are obtained. $K_I(g)$ is calculated taking the illuminated area 0.6 cm^2 and the TiO_2 weight per cm^2 layer, $W_A = D_{350}/\epsilon_A^{350} = 0.32$ mg/cm^2. Figure 5 yields $K_I(g) = 2.2 \times 10^3$ $s^{1/2}$ $g^{3/2}$ $ein^{-1/2}$ based on $\epsilon_A^{350} = 2.91$ mg^{-1} cm^2 for STS-01 TiO_2. Similarly, $K_I(V)$ is calculated using the layer thickness $l = D_{350}/(\epsilon_{350}[TiO_2]) = 0.93/(244 \times 35.2) = 1.08 \times 10^{-4}$ cm, where ϵ_{350} has the usual meaning in units of M^{-1} cm^{-1}, yielding $K_I(V) = K_I V^{1/2} = 1.6 \times 10^5 \times (6.5 \times 10^{-5})^{1/2} = 1.3 \times 10^3$ $s^{1/2}$ $cm^{3/2}$ $ein^{-1/2}$. Table 1 shows that the values of $K_I(g)$ and $K_I(V)$ do not change with wavelength, while K_I ($s^{1/2}$ $ein^{-1/2}$) does.

Since the porosity of different titania may differ, it is preferable to refer to the absorbed photon density in terms of ein g^{-1} s^{-1}, which does not require knowledge of the porosity. This makes possible the comparison between layers and dispersed forms of TiO_2 such as sols, suspensions, and powders.

Note that, under the conditions of Figure 5 and Table 1, the light intensity hitting the layer is about 7 times higher than the transmitted light intensity. Under actual conditions of most works on TiO_2 layers, powders, and suspensions photocatalysis, the quantum yield varies with distance within the illuminated medium. A more rigorous treatment should involve the absorbed light distribution within the active medium. This distribution along the light path is given by the Lambert−Beer equation. The quantum yield increases along the light path within the activated volume, as the absorbed photon density decreases. The quantum yield in an infinitesimal sublayer with unit cross-section and thickness dl at a distance l from the layer's front edge is given by $\Phi_l = \Phi_{max}/(1 + K_d I_{d,l}^{1/2})$, where $I_{d,l}$ is the absorbed photon density by the infinitesimal sublayer between distance l and $l + dl$. K_d ($s^{1/2}$ $g^{1/2}$ $ein^{-1/2}$) differs from $K_I(g)$ and $K_I(V)$ because it is related to a sufficiently thin layer, where the absorbed photon density can be considered uniform. In contrast, $K_I(g)$ and $K_I(V)$ represent the respective parameters calculated

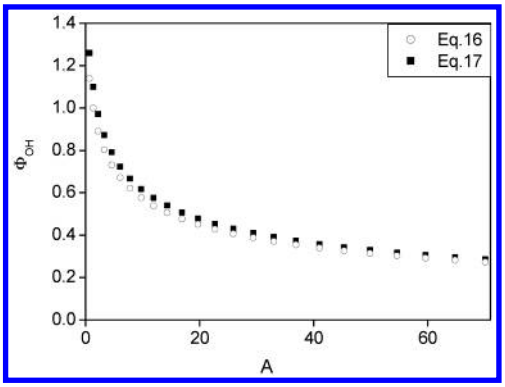

Figure 6. Dependence of Φ_{OH} on *A*. Φ_{OH} (including hydroxyl radicals produced by reduction of H_2O_2) calculated according to eqs 16 and 17, respectively. STS-01, $D = 1.0$, $\epsilon_A = 4360$ cm^2/g, $K_d = 1640$ s$^{1/2}$ g$^{1/2}$ ein$^{-1/2}$, I_0: from 2.5×10^{-11} ein cm^{-2} s^{-1} to 2.0×10^{-9} ein cm^{-2} s^{-1}.

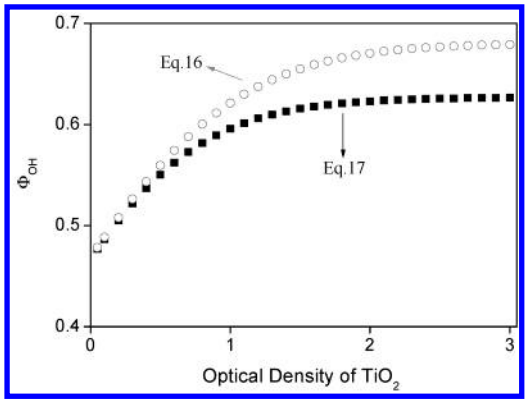

Figure 7. Dependence of Φ_{OH} on the TiO_2 absorbance. Φ_{OH} (including hydroxyl radicals produced by reduction of H_2O_2) calculated according to eqs 16 and 17, respectively. STS-01, $\epsilon_A = 4360$ cm^2/g, $K_d = 1640$ s$^{1/2}$ g$^{1/2}$ ein$^{-1/2}$, $I_0 = 4.0 \times 10^{-10}$ ein cm^{-2} s^{-1}.

on the basis of the arithmetic average photon density. Thus, unlike $K_l(g)$ and $K_l(V)$, K_d is a photocatalytic constant of the TiO_2. It is related to the efficiency of electron hole recombination relative to surface water oxidation to hydroxyl radicals, at the given pH and oxygen concentration. Note that K_d is not a simple ratio of the respective rate constants, as the recombination rate depends on all reactions of electrons and holes.

From Beer's law, the absorbed light intensity (ein cm^{-2} s^{-1}) between distance l and $l + dl$, $I_{a,l} = -dI_{t,l} = -d(I_0 \times 10^{-\epsilon[TiO_2]l}) = 2.303\epsilon I_0[TiO_2]10^{-D}dl$, where the $I_{t,l}$ is the transmitted light intensity at distance l, which is also the incident light intensity for the sublayer. Replacing $D = [TiO_2]\epsilon l$ by $D = \epsilon_A W_A$, one obtains: $I_{a,l} = -dI_{t,l} = -d(I_0 \times 10^{-\epsilon_A W_A}) = 2.303\epsilon_A I_0 \times 10^{-D}dW_A$. The absorbed photon density (ein g^{-1} s^{-1}) at the sublayer, $I_{d,l} = 2.303\epsilon_A I_0 \times 10^{-D}$. Inserting $I_{d,l}$ in the above Φ_l equation yields: $\Phi_l = \Phi_{max}/(1 + K_d(2.303\epsilon_A I_0 \times 10^{-D})^{1/2})$. The observed quantum yield $\Phi_{exp} = R/I_a$, is the weighted average of the quantum yields along the light path within the active medium. R is the overall rate of product formation, and I_a is the total absorbed light intensity (ein s^{-1} cm^{-2}).

$$\Phi_{exp} = R/I_a = I_a^{-1}\int_0^{W_A}\Phi_l I_{a,l} = (I_0(1 - 10^{-D}))^{-1}\int_0^{W_A}\{(2.303\Phi_{max}\epsilon_A I_0 \times 10^{-\epsilon_A W_A})/[1 + K_d(2.303\epsilon_A I_0 \times 10^{-\epsilon_A W_A})^{0.5}]\}dW_A \quad (15)$$

The integration yields

$$\Phi_{exp} = 2\Phi_{max}(A^{0.5}(1 - 10^{-0.5D}) + \ln[(1 + A^{0.5} \times 10^{-0.5D})/(1 + A^{0.5})])/A(1 - 10^{-D}) \quad (16)$$

where $A = 2.3K_d^2\epsilon_A I_0$. This equation enables the determination of K_d. The above equation, however, is not convenient to use. Therefore we introduce a simplified relation where instead of the weighted average values of Φ_l, the quantum yield is calculated as yield corresponding to the weighted average of $I_{d,l}^{1/2}$, namely, the integral of $(I_{d,l})^{1/2}I_{a,l}/I_a$. The integration yields: $(I_{d,l}^{1/2})_w = I_a^{-1}\int(I_{d,l})^{1/2}I_{a,l} = 2 \times (2.3\epsilon_A I_0)^{0.5}(1 - 10^{-1.5D})/3(1 - 10^{-D})$, and hence

$$\Phi_{exp} = \Phi_{max}/(1 + K_d(I_{d,l}^{1/2})_w) = \Phi_{max}/(1 + 2A^{0.5}(1 - 10^{-1.5D})/3(1 - 10^{-D})) \quad (17)$$

Comparison between the Two Formulas. Figures 6 and 7 show the comparison between the two equations with variables *A* and *D*, respectively. Clearly, the differences between the exact and approximate treatments are relatively small. Similarly, derivation of K_d using both equations shows differences up to 4% only, under the experimental conditions of the present work. This justifies the use of the simplified equation to calculate K_d. The effects of light intensity, light distribution, and thickness of the active medium, as well as wavelength (light density) are taken into account in the evaluation of K_d. Therefore K_d is directly related to the nature of the TiO_2 and its photocatalytic efficiency. K_d is inversely proportional to the photocatalytic efficiency, namely, when two different titania preparations are compared, the one with the lower K_d value shows a lower decrease of •OH quantum yield upon increasing the light intensity.

Comparison with Other Work in Dilute Aqueous Suspensions. According to the theoretical model of Grela et al.,[71] bimolecular carrier recombination does not follow second-order kinetics, and therefore no square root dependency of the yield vs light intensity is expected if reaction 3 involves the primary carriers. This implies that the reactants in reaction 3 are secondary intermediates such as electrons and holes trapped at inter nanoparticle boundaries. Under the conditions of Figure 5, an average of 0.15 and 15 photons/s are absorbed at the lowest and highest intensities, respectively, by the STS-01 TiO_2. Since the quantum yield in this range varies from 1 to about 0.2, an average of 0.15−3 electron−hole pairs are produced per second in each nanoparticle. This frequency is much smaller than required for any measurable fraction of the primary carriers to react at the TiO_2−solution interface. It is unlikely that the electron−hole pairs build up to concentrations sufficiently high for showing second-order time profiles if their reactions are confined to a single nanocrystallite. The observed square root dependency at very low intensities implies that the microvolume, which is significant for the recombination process, is much larger than the volume around the nanocrystallite where the intermediates have been initially produced. Reactions involving secondary products such as reactions 5, 6, 18, and 19 take place with adsorbed and possibly bulk reactants, which migrate within the layer.

Quantum yield of the same order, independent of absorbed light intensity, has been reported for aqueous suspensions of TiO_2 (Degussa P-25), under similar photon flux, although the absorbed photon densities and intermediate concentrations differ by several orders of magnitude.[14] Differences between nanoparticle layers and suspended particles may have opposite effects on the rates of the second-order recombination. The intraparticle reactions in the suspensions take place in the ultra-small domain

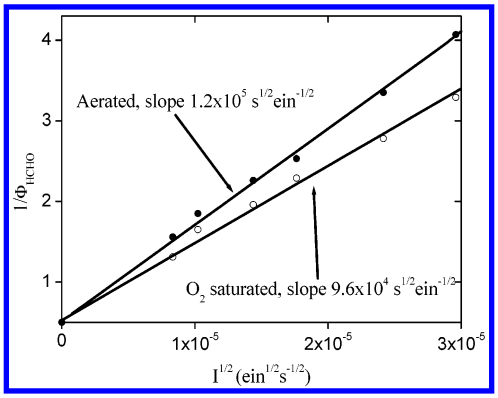

Figure 8. Effect of oxygen on the quantum yield of HCHO. STS-21, 340 nm, pH 7 (0.002 M Na_2HPO_4, 0.002 M NaH_2PO_4), using 2 M CH_3OH, $D_{layer}^{340} = 0.98$. Φ_{OH} includes OH radicals obtained via reduction of O_2.

of a single nanoparticle (or aggregate), while the entire volume of the water is available for reactions of bulk intermediates. On the other hand, interparticle reactions of intermediates produced at different nanocrystallites in dilute suspensions are expected to be relatively very slow, in contrast to layers. Thus, part of the back reactions in the suspensions are faster than in the layer due to the restricted small reaction volume, while reactions involving intermediates in the bulk are faster in the layer because of the much smaller volume of the active solution. No quantitative comparison is possible due to unknown kinetic parameters and incomplete scavenging of the hydroxyl radical.

Oxygen Effect. Although in the absence of specific information on the various kinetic rate constants it is not possible to carry out quantitative kinetic analysis, the results can be rationalized on the basis of the known nature of the involved intermediates. The dependence of $\Phi_{product}$ on scavenger concentration (Figure 4 and ref.[49]), reflects competition between reactions 7 and 13. Reaction 13 represents reduction of $^{\bullet}OH$ by $e_{TiO_2}^-$, $^{\bullet}RH$, or $O_2^{-\bullet}/HO_2^{\bullet}$, and is completely suppressed at sufficiently high scavenger concentration. The limiting yield, which is smaller than the maximum of $\Phi_{product} = 2$, is directly related to the yield of $^{\bullet}OH$ radicals. The latter is determined by the competition between reactions 2 and 3. This competition is affected by O_2, $HO_2^{\bullet}/O_2^{-\bullet}$ (produced by oxygen reduction according to reactions 4, 8, and 9), and H_2O_2 produced by further reduction of the superoxide radicals (reactions 5 and 11). The reduction of oxygen by the organic radicals (reactions 8 and 9) are much faster than by $e_{TiO_2}^-$ (reaction 4).[17] Consequently the predominant effect of oxygen on the $^{\bullet}OH$ yield is through the supply of $HO_2^{\bullet}/O_2^{-\bullet}$ and H_2O_2, which suppress the steady-state concentration of the electrons. H_2O_2 yields additional $^{\bullet}OH$ radicals upon subsequent reduction (reaction 6). The effect of oxygen concentration at various light intensities is shown in Figure 8 for air- and oxygen-saturated solutions, respectively. The effect of 5-fold increase in oxygen concentration is relatively small, amounting to only 25% increase of the product yield at high light intensities. Note that since the intercept in Figure 6 is 0.5, the relative effect of oxygenation depends on light intensity. Measurements with other TiO_2 preparations show similar results, with the effect of oxygenation on Φ_{HCHO} up to 30%.

The relatively small effect of oxygen is not surprising in view of the parallel reaction such as 5, 6, 18, and 19, which affect the overall electron hole recombination but do not involve molecular oxygen. In addition, the surface concentration of oxygen may not increase linearly with its bulk concentration if

TABLE 2: Effect of Oxygen Concentration on Formaldehyde Yield; 3 mL of 2 M CH_3OH Solution in a 5 mL Cell, Illuminated 60 min, Light Dimensions 0.3 × 1.5 cm^2

TiO_2 type	saturating gas	pH	I_{abs} (ein/min)	$\lambda_{illumination}$ (nm)	Φ_{HCHO}
STS-01[a]	argon	6[b]	3.2×10^{-9}	333	~0.035
STS-01[a]	air	6[b]	3.2×10^{-9}	333	0.54
STS-01[a]	O_2	6[b]	3.2×10^{-9}	333	0.69

[a] Layer on ITO, $D^{333} = 0.80$ in the solution (spectrophotometer). [b] 0.002 M Na_2HPO_4, 0.020 M NaH_2PO_4.

TiO_2 surface saturation by oxygen is approached in the air-saturated systems.

$$h^+ + O_2^{-\bullet}/HO_2^{\bullet} \rightarrow O_2 \qquad (18)$$

$$h^+ + H_2O_2 \rightarrow H^+ + HO_2^{\bullet}/O_2^{-\bullet} \qquad (19)$$

Table 2 shows a similar oxygen effect, with 28% increase in Φ_{HCHO} upon saturation with oxygen, using STS-01 TiO_2 at pH 6.

In conclusion, reactions 4 and 9 (or 4, 8, and 10 in the respective methanol systems), followed by reactions 5 and 6, provide a chain mechanism for removing the TiO_2 electrons. The specific rates of these reactions affect the steady-state concentration of electrons, which escape the fast reaction 3. Although the net yield of H_2O_2 is relatively small under all conditions (Figure 3), implying efficient removal of H_2O_2 by reactions 6 and 12, the difference between the methanol and HCO_2H/HCO_2^- systems implies that part of the organic free radicals $^{\bullet}CO_2^-$ (and possibly $^{\bullet}CH_2OH$) react with H_2O_2 despite the presence of excess oxygen.

Reactions 18 and 19 had to be invoked in order to simulate the formation of HCHO (or CO_2) and H_2O_2 and the effect of oxygen, using literature rate constants[17,72,73] whenever available. No quantitative information could be obtained from such simulations because of too many uncertainties concerning reaction rate constants and distribution of intermediates and products such as HO_2/O_2^- and H_2O_2 between the layer and the bulk of solution.

Discussion of the Lack of pH Effect. The redox potentials of the species involved in the competing reactions 2 and 3, which directly determine the yield of the $^{\bullet}OH$ radical, change with pH in a way that the driving forces for these reactions remain unchanged. The same applies to the driving force of reaction 6. On the other hand, the driving forces for reactions 4 and 5, which affect the $^{\bullet}OH$ yield indirectly, vary with pH in opposite directions, and so is the case with reactions 18 (reactant O_2^-) and 19. Thus, the lack of pH effect on the yield of the $^{\bullet}OH$ radical is conceivable on the basis of the proposed mechanism.

Different TiO_2 Preparations and Particle Size. It is commonly assumed that the properties of TiO_2 nanocrystallites strongly depend on accidental impurities and may change by minor uncontrolled variation of conditions. In view of this, conclusions based on different TiO_2 samples, particularly if prepared according to different procedures or in different laboratories, are considered not very reliable. However, the results of Table 3 show a striking similarity of the K_I values for all the TiO_2 preparations, although they differ in technique, pH, stabilization conditions, and particle size.

K_d is related to the photocatalytic efficiency, namely, the rate of reaction 2 relative to the competing hole-reduction reactions 3, 18, and 19. The relatively small variation of K_d implies that

TABLE 3: Comparison between Different TiO_2 Preparations K_I and Φ_{max} Determined from the Slope and Intercept of Figures Similar to (5), Using 3 mL of 2 M CH_3OH Solution at pH 6 in a 5 mL Cell, Illuminated 60 min, with Light Dimensions 0.4 × 1.5 cm^2. Layer Absorbance, $D^{340} = 1$

sample number[a]	1	2	3	4	5	6	7	8
sample name	300A	300B	P-25	STS-01	STS-21	self-made TiO_2 by sol−gel	nanotubes	pellets
$10^{-5}K_I$ ($s^{1/2}$ $ein^{-1/2}$)	1.7	1.6	1.9	1.6	1.7	2.6	2.2	1.7
$10^{-3} \times K_d$ ($s^{1/2}$ $g^{1/2}$ $ein^{-1/2}$)	2.2	2.0	1.5	2.0	1.6	3.5	1.9	2.4
Φ_{max} (HCHO)	1.9	1.9	1.7	2.0	1.9	1.9	1.9	1.8

[a] See Experimental Section.

the TiO_2 system is relatively simple provided that limiting concentrations of substrates are employed, and corrections for light scattering and inhomogeneity of photon density are introduced. Reactions 5, 11, 12, and 18 involve superoxide radicals, which are produced by oxygen reduction by $e_{TiO_2}^-$ and the organic radical $RH^\bullet$. In the cases of methanol and formate/formic acid, the latter radical reacts with oxygen and produces superoxide radicals. In this case, derivation of Φ_{OH} is simple, since the product yield (HCHO or CO_2) depends only little, if at all, on the nature of the organic substrate. However, many organic molecules produce peroxyl radicals, which do not give rise to superoxide. These radicals may show specific reaction rates toward electrons and holes, and therefore product yields may differ from those reported in the present work. Furthermore, peroxyl radicals that are not decomposed to superoxide radicals are likely to show differences between different organic solutes, even when all the $^\bullet OH$ radicals are scavenged by the organic solute.

Obviously, large differences between various types of "photocatalytic" TiO_2 are expected at low substrate concentrations, when competition between reactions 7 and 13 may be important. Under such conditions, the photocatalytic efficiency depends on substrate reactivity toward $^\bullet OH$ radicals as well as on adsorption to the TiO_2 surface, and smaller particles with overall large surface area will prove to be more effective per unit weight.

The lack of a pronounced effect of particle size under our conditions means that the competition between the oxidation of water by reaction 2 and reduction of the holes depends little, if at all, on particle size. The rate of reaction 2 is not expected to depend on particle size, because the rate of electron transfer through the TiO_2/water interface is only little affected by the size.[74−76] This conclusion applies to reduction of adsorbed oxygen and its intermediates as well as interfacial electron transfer to the holes from adsorbed molecules. Note that in an earlier publication slower reduction rates have been reported for TiO_2 particles of 1 nm diameter.[17] The 1-nm particles have been freshly prepared and stored at low temperature in colloid solution, and the spectrum of the electron was different from that observed in larger (5 nm diameter) particles. These results do not reflect to the present comparison between particles with dimensions of at least several nanometers, which have been aged for many months at room temperature.

The rate of the recombination reaction 3 does not depend on particle size under our conditions, because the comparison between different TiO_2 in the present work involves the same number of absorbed photons per unit volume. Therefore, the competition between reactions 2 and 3 is not expected to depend on size. The actual situation, however, may be more complicated if surface-trapped electrons are involved, because the surface concentration is proportional to particle radius.

Conclusions

The yield of $^\bullet OH$ has been determined in TiO_2 nanocrystallite layers and suspensions using methanol and formic acid/formate as scavengers. The free radical produced from methanol reacts with oxygen, quickly producing superoxide radicals at pH > 6 (phosphate buffer). The formation of superoxide radicals slows down at acid pH. In the formic acid/formate system, superoxide radicals are efficiently produced in the presence of oxygen in the entire pH range. At high scavenger concentration, the limiting yield of $^\bullet OH$ does not depend on the nature of the scavenger as long as the peroxy intermediate quickly dissociates to the superoxide radical. Φ_{OH} shows the well-known square root dependency on the absorbed light intensity and depends on oxygen concentration, although the difference between air- and oxygen-saturated solutions is relatively small. Hydrogen peroxide competes efficiently with oxygen for the TiO_2 electrons, and only negligible steady-state concentration of hydrogen peroxide builds up.

A constant, K_d, directly related to the photocatalytic efficiency of TiO_2 at a given pH and O_2 concentration, under limiting substrate concentration has been defined. This parameter is a property of the TiO_2. It involves a correction for light distribution and does not depend on the specific experimental conditions such as light intensity, wavelength, and thickness of the active medium.

In large nanocrystallite systems, which have been allowed to age sufficient time to minimize surface imperfections, the yield of $^\bullet OH$ radicals depends relatively little on the specific TiO_2 preparation, particle size, and pH, under otherwise similar conditions.

The results are rationalized in terms of a simple competition between recombination of electrons and holes and surface water oxidation. Oxygen, although reacting with electrons relatively slowly, removes electrons, converting them to superoxide radicals. The superoxide radicals are further reduced to H_2O_2, or oxidized by holes. Reduction of superoxide radicals enhances the generation of $^\bullet OH$ radicals, while superoxide oxidation by holes has the opposite effect. Hydrogen peroxide can also react with both electrons and holes. Thus, the yield of $^\bullet OH$ radicals depends on the specific reaction rates of the above intermediates. Although these rates are not known for all the relevant reactions, the net product yield is the same for different organic photooxidation as long as the limiting yields are concerned (at a given light intensity), and the predominant oxygen intermediate (besides the hydroxyl radical) is the superoxide radical (as opposed to the organic peroxyl radical).

The present work indicates that the fundamental processes in TiO_2 photocatalysis are simple, and a general oxidation mechanism may apply to different TiO_2 preparations, with only little effect of pH and particle size. More work is required to determine the missing kinetic parameters. The resulting unified kinetic treatment under standard conditions will enable us to predict product yields from the available adsorption data, $^\bullet OH$ rate constants, and knowledge of peroxyl chemistry (in systems which do not generate the superoxide radicals).

Acknowledgment. We are indebted to E. Gilead and Y. Ozeri for technical assistance. We acknowledge the support by

the European Commission RTD framework 6-th program and the Israel Ministry of Science. We thank Millenium Inorganic Chemicals, Degussa, and Sachtleben Chemie companies and Profs. Fujishima and Gedanken for supplying titania samples.

References and Notes

(1) Gerischer, H. *Photochem. Photobiol.* **1972**, *16*, 243−260.
(2) Fujishima, A.; Honda, K. *Bull. Chem. Soc. Jpn.* **1971**, *44*, 1148.
(3) Hoffmann, M. R.; Martin, S. T.; Choi, W.; Bahnemann, D. W. *Chem. Rev.* **1995**, *95*, 69−96.
(4) Serpone, N.; Khairutdinov, R. F. *Semicond. Nanoclusters, Phys. Chem. Catalytic Aspects* **1997**, *103*, 417−444.
(5) Pelizzetti, E.; Minero, C. *Colloids Surf. Physicochem. Eng. Aspects* **1999**, *151*, 321−327.
(6) Mills, A.; Davies, R. H.; Worsley, D. *Chem. Soc. Rev.* **1993**, *22*, 417−425.
(7) Ollis, D. F.; Turchi, C. *Environ. Prog.* **1990**, *9*, 229−234.
(8) Fox, M. A.; Dulay, M. T. *Chem. Rev.* **1993**, *93*, 341−357.
(9) Fujishima, A.; Hashimoto, K.; Watanabe, T. *TiO_2 Photocatalysis Fundamentals and Applications*, 1st ed.; BKC, Inc.: Tokyo, 1999.
(10) Goldstein, S.; Czapski, G.; Rabani, J. *J. Phys. Chem.* **1994**, *98*, 6586−6591.
(11) Jaeger, C. D.; Bard, A. J. *J. Phys. Chem.* **1979**, *83*, 3146−3152.
(12) Harbour, J. R.; Chow, V. S. F.; Bolton, J. R. *Can. J. Chem.* **1974**, *52* (2), 3549.
(13) Buxton, G. V.; Greenstock, C. L.; Helman, W. P.; Ross, A. B. *J. Phys. Chem. Ref. Data* **1988**, *17*, 513−886.
(14) Grela, M. A.; Coronel, M. E. J.; Colussi, A. J. *J. Phys. Chem.* **1996**, *100*, 16940−16946.
(15) Riegel, G.; Bolton, J. R. *J. Phys. Chem.* **1995**, *99*, 4215−4224.
(16) Schwarz, P. F.; Turro, N. J.; Bossman, S. H.; Braun, A. M.; Abdel Wahab, A. A.; Duerr, H. *J. Phys. Chem.* **1997**, *101*, 7127−7134.
(17) Gao, R.; Safrany, A.; Rabani, J. *Radiat. Phys. Chem.* **2003**, *67*, 25−39.
(18) Aguado, M. A.; Anderson, M. A.; Hill, C. G. *J. Mol. Catal.* **1994**, *89*, 165−178.
(19) Bahnemann, D.; Bockelmann, D.; Goslich, R. *Sol. Energy Mater.* **1991**, *24*, 564−583.
(20) Bideau, M.; Claudel, B.; Faure, L.; Kazouan, H. *J. Photochem. Photobiol. A−Chem.* **1991**, *61*, 269−280.
(21) Horikoshi, S.; Hidaka, H.; Serpone, N. *J. Photochem. Photobiol. A−Chem.* **2001**, *138*, 69−77.
(22) Inel, Y.; Okte, A. N. *J. Photochem. Photobiol. A−Chem.* **1996**, *96*, 175−180.
(23) Inel, Y.; Okte, A. N. *Chemosphere* **1998**, *36*, 2969−2975.
(24) Lepore, G. P.; Pant, B. C.; Langford, C. H. *Can. J. Chem.−Rev. Can. Chim.* **1993**, *71*, 2051−2059.
(25) Martino, D. M.; vanWilligen, H.; Spitler, M. T. *J. Phys. Chem. B* **1997**, *101*, 8914−8919.
(26) Mills, A.; Belghazi, A.; Davies, R. H.; Worsley, D.; Morris, S. *J. Photochem. Photobiol. A−Chem.* **1994**, *79*, 131−139.
(27) Ohko, Y.; Hashimoto, K.; Fujishima, A. *J. Phys. Chem. A* **1997**, *101*, 8057−8062.
(28) Ohko, Y.; Tryk, D. A.; Hashimoto, K.; Fujishima, A. *J. Phys. Chem. B* **1998**, *102*, 2699−2704.
(29) Preis, S.; Terentyeva, Y.; Rozkov, A. *Water Sci. Technol.* **1997**, *35*, 165−174.
(30) Sanchez, L.; Peral, J.; Domenech, X. *Electrochim. Acta* **1996**, *41*, 1981−1985.
(31) Schwarz, P. F.; Turro, N. J.; Bossmann, S. H.; Braun, A. M.; Wahab, A.; Durr, H. *J. Phys. Chem. B* **1997**, *101*, 7127−7134.
(32) Serpone, N.; Sauve, G.; Koch, R.; Tahiri, H.; Pichat, P.; Piccinini, P.; Pelizzetti, E.; Hidaka, H. *J. Photochem. Photobiol. A−Chem.* **1996**, *94*, 191−203.
(33) Serra, F.; Trillas, M.; Garcia, J.; Domenech, X. *J. Environ. Sci. Health Part A−Environ. Sci. Eng. Toxic Hazard. Subst. Control* **1994**, *29*, 1409−1421.
(34) Sharma, B. K.; Vardia, J.; Rao, P.; Ameta, S. C. *Hung. J. Ind. Chem.* **1998**, *26*, 1−5.
(35) Stafford, U.; Gray, K. A.; Kamat, P. V. *J. Catal.* **1997**, *167*, 25−32.
(36) Uchihara, T.; Asato, Y.; Kinjo, A. *J. Photochem. Photobiol. A−Chem.* **1992**, *67*, 101−107.
(37) Nosaka, Y.; Fox, M. N. *Langmuir* **1987**, *3*, 1147−1150.
(38) Nosaka, Y.; Fox, M. A. *J. Phys. Chem.* **1986**, *90*, 6521−6522.
(39) Hellouin, Y.; Viktorovitch, P. *Jpn. J. Appl. Phys. Part 1−Regul. Pap. Short Notes Rev. Pap.* **1998**, *37*, 466−470.
(40) Gerischer, H. *Electrochim. Acta* **1995**, *40*, 1277−1281.
(41) Hoffman, A. J.; Carraway, E. R.; Hoffmann, M. R. *Environ. Sci. Technol.* **1994**, *28*, 776−785.
(42) Ameta, S.; Meta, M.; Sharma, B.; Dak, M. *Izv. Vyss. Uchebnykh Zaved. Khim. Khimichesk. Tekhnol.* **1994**, *37*, 43−47.
(43) Hoffman, A. J.; Yee, H.; Mills, G.; Hoffmann, M. R. *J. Phys. Chem.* **1992**, *96*, 5540−5546.
(44) Shiragami, T.; Fukami, S.; Wada, Y. J.; Yanagida, S. *J. Phys. Chem.* **1993**, *97*, 12882−12887.
(45) Rabani, J.; Klug-Roth, D.; Henglein, A. *J. Phys. Chem.* **1974**, *78*, 2089−2093.
(46) Behar, D.; Czapski, G.; Rabani, J.; Dorfman, L. M.; Schwarz, H. A. *J. Phys. Chem.* **1970**, *74*, 3209−3213.
(47) Rabani, J.; Nielsen, S. O. *J. Phys. Chem.* **1969**, *73*, 3736−3744.
(48) Perissinotti, L. L.; Brusa, M. A.; Grela, M. A. *Langmuir* **2001**, *17*, 8422−8427.
(49) Gao, R.; Stark, J.; Bahnemann, D. W.; Rabani, J. *J. Photochem. Photobiol. A: Chemistry* **2002**, *148*, 387−391.
(50) Nazeeruddin, M. K.; Kay, A.; Rodicio, I.; Humphry-Baker, R.; Muller, E.; Liska, P.; Vlachopoulos, N.; Graetzel, M. *J. Am. Chem. Soc.* **1993**, *115*, 6382−6390.
(51) Wang, Y. Q.; Tang, X. H.; Yin, L. X.; Huang, W. P.; Hacohen, Y. R.; Gedanken, A. *Adv. Mater.* **2000**, *12*, 1183−1186.
(52) Nash, T. *Biochemistry* **1953**, *55*, 416−421.
(53) Hatchard, C. G.; Parker, C. A. *Proc. R. Soc. Ser. A* **1956**, *235*, 518−536.
(54) Demas, J. N.; Bowman, W. D.; Zalewski, E. F.; Valapoldl, R. A. *J. Phys. Chem.* **1981**, *85*, 2766−2771.
(55) Salinaro, A.; Emeline, A. V.; Zhao, J.; Hidaka, H.; Ryabchuk, V. K.; Serpone, N. *Pure Appl. Chem.* **1999**, *71*, 321−355.
(56) Brandi, R. J.; Alfano, O. M.; Cassano, A. E. *Environ. Sci. Technol.* **2000**, *34*, 2623−2630.
(57) Serpone, N.; Salinaro, A. *Pure Appl. Chem.* **1999**, *71*, 303−320.
(58) Brandi, R. J.; Alfano, O. M.; Cassano, A. E. *Environ. Sci. Technol.* **2000**, *34*, 2631−2639.
(59) Davydov, L.; Smirniotis, P. G. *J. Catal.* **2000**, *191*, 105−115.
(60) Kesselman, J. M.; Weres, O.; Lewis, N. S.; Hoffmann, M. R. *J. Phys. Chem. B* **1997**, *101*, 2637−2643.
(61) Adams, G. E.; Boag, J. W.; Currant, J.; Michael, B. D. In *Pulse Radiolysis*; Ebert, M., Keene, J. P., Swallow, A. J., Baxendale, J. H., Eds.; Academic Press: New York, 1965; pp 131−143.
(62) Willson, R. L.; Greenstock, C. L.; Adams, G. E.; Wageman, R.; Dorfman, L. M. *Int. J. Radiat. Phys. Chem.* **1971**, *3*, 211−220.
(63) Bates, S. P.; Kresse, G.; Gillan, M. J. *Surf. Sci.* **1998**, *409*, 336−349.
(64) Kackell, P.; Terakura, K. *Surf. Sci.* **2000**, *461*, 191−198.
(65) Liao, L. F.; Wu, W. C.; Chen, C. Y.; Lin, J. L. *J. Phys. Chem. B* **2001**, *105*, 7678−7685.
(66) Adams, G. E.; Boag, J. W.; Michael, B. D. *Trans. Faraday Soc.* **1965**, *61*, 1417−1424.
(67) Gerischer, H. *Electrochim. Acta* **1993**, *38*, 3−9.
(68) Wang, C. Y.; Rabani, J.; Bahnemann, D. W.; Dohrmann, J. K. *J. Photochem. Photobiol. A−Chem.* **2002**, *148*, 169−176.
(69) Kormann, C.; Bahnemann, D. W.; Hoffmann, M. R. *Environ. Sci. Technol.* **1991**, *25*, 494.
(70) Ollis, D. F.; Pelizzetti, E.; Serpone, N. *Environ. Sci. Technol.* **1991**, *25*, 1523.
(71) Grela, M. A.; Colussi, A. J. *J. Phys. Chem.* **1996**, *100*, 18214−18221.
(72) Rothenberger, G.; Moser, J.; Graetzel, M.; Serpone, N.; Sharma, D. K. *J. Am. Chem. Soc.* **1985**, *107*, 8054−8059.
(73) Serpone, N.; Lawless, D.; Khairutdinov, R.; Pelizzetti, E. *J. Phys. Chem.* **1995**, *99*, 16655−16661.
(74) Zang, L.; Rodgers, M. A. J. *J. Phys. Chem. B* **2000**, *104*, 468−474.
(75) Brown, G. T.; Darwent, J. R.; Fletcher, D. I. *J. Am. Chem. Soc.* **1985**, *107*, 6446−6451.
(76) Gao, R.; Safrany, A.; Rabani, J. *Radiat. Phys. Chem.* **2002**, *65*, 599−605.